

Supporting Information

Aqueous TMAO Solution under High Hydrostatic Pressure

Inga Kolling,[†] Christoph Hölzl,[‡] Sho Imoto,[‡] Serena R. Alfarano,[†] Hendrik Vondracek,[†] Lukas Knake,[†] Federico Sebastiani,[†] Fabio Novelli,[†] Claudius Hoberg,[†] Jean-Blaise Brubach,[¶] Pascale Roy,[¶] Harald Forbert,[§] Gerhard Schwaab,^{*,†} Dominik Marx,^{*,‡} and Martina Havenith^{*,†}

[†]*Lehrstuhl für Physikalische Chemie II, Ruhr-Universität Bochum, 44780 Bochum, Germany*

[‡]*Lehrstuhl für Theoretische Chemie, Ruhr-Universität Bochum, 44780 Bochum, Germany*

[¶]*Ligne AILES à Synchrotron SOLEIL, L'Orme des Merisiers, F-91192 Gif-sur-Yvette, France*

[§]*Center for Solvation Science ZEMOS, Ruhr-Universität Bochum, 44780 Bochum, Germany*

E-mail: gerhard.schwaab@rub.de; dominik.marx@theochem.ruhr-uni-bochum.de;
martina.havenith@rub.de

Experimental Setup

Details of the experimental setup have been reported in recent papers by our group.¹⁻³ In short, Fourier transform spectra of ultrapure water and aqueous TMAO solutions up to 12 kbar were recorded in the frequency range 40-420 cm^{-1} using a commercial FTIR spectrometer (Bruker Vertex 80V, Bruker, Ettlingen, Germany). It is equipped with a mercury vapor lamp as a source, a 6x beam condenser (Pike Technologies, Madison, WI, USA) and an external liquid He-cooled bolometer (HDL-5, Infrared Laboratories, Inc., Tucson, AZ, USA) as a detector. For our measurements, we used a commercially available Diamond Anvil Cell [DAC] (Almax EasyLab VivoDAC, Almax EasyLab, Diksmuide, Belgium), consisting of a diamond anvil and a flat diamond window. Brass rings with an outer diameter of 3.95 mm, an inner diameter of 0.5 mm and a thickness of approximately 40 μm , as manufactured by LMB Automation (Iserlohn, Germany), were used without any pre-indentation. Ultrapure water (ASTMI, TKA Wasseraufbereitungssysteme, Niederelbert, Germany) or aqueous TMAO solution was filled into the hole of the gasket. For the measurements in Bochum, the DAC was closed with a torque of 3.5 Nm, applied by a torque wrench. The measurements at the SOLEIL facility⁴ were carried out with a 30 μm thick cell. A ruby sphere was placed inside the cell for internal pressure determination of the solution via ruby fluorescence. All spectra were recorded with a resolution of 1 cm^{-1} , averaging over 64 datasets. The DAC was pressurized utilizing a gas membrane using an automated pressurizing system (Pace 5000, GE Measurement, Billerica, MA, USA). To achieve pressure equilibration inside the sample volume, spectra were recorded three minutes after the membrane pressure was changed. The thickness of the sample cell as a function of gas membrane pressure was measured *ex-situ* using two confocal distance sensors (Micro-Epsilon IFS 2403, Micro-Epsilon, Ortenburg, Germany), focused on the outer diamond windows of the DAC. All our experimental analyses have been performed using Mathematica 12 (Wolfram Research, Champaign, IL, USA). Details on the pressure calibration and thickness determination for the Bochum measurements can be found elsewhere.^{2,3}

Experimental Data Analysis

Principal Component Analysis (PCA)

In the following, we describe the data analysis for membrane and internal pressure as well as the changes in the thickness of the cell of TMAO solution data.

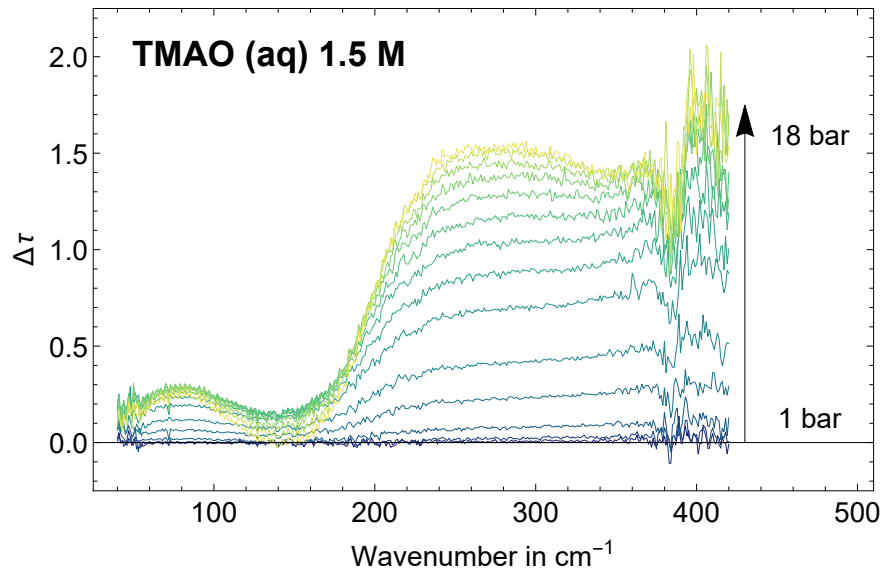


Figure 1: Difference in optical depths $\Delta\tau$ of 1.5 M aqueous TMAO solutions as a function of membrane pressure. The TMAO solution at ambient pressure was used as reference.

For the data analysis of the pure water and TMAO solution spectra, we used $\Delta\tau$ as observable, the difference in optical depth, i.e., the negative logarithm of the transmission ratio between the pressure (p) dependent intensity of the transmission I_{sample} with respect to a reference I_{ref} at ambient pressure p_0 :

$$\Delta\tau = -\ln\left(\frac{I_{\text{sample}}(\tilde{\nu}, p)}{I_{\text{ref}}(\tilde{\nu}, p_0)}\right) = \alpha_{\text{sample}}(\tilde{\nu}, p)d(p) - \alpha_{\text{ref}}(\tilde{\nu}, p_0)d(p_0) \quad (1)$$

As shown in equation 1, $\Delta\tau$ is the difference between the product of the absorption coefficient α times the cell thickness d at a given pressure and the product at ambient pressure as a reference. In Figure 1 we plot the observable $\Delta\tau$ as function of membrane pressure p_{memb} for 1.5 M aqueous TMAO solutions in a cell with the thickness $d(p_0) = 40 \mu\text{m}$. For further

analysis we performed a principal component analysis of $\Delta\tau(\tilde{\nu}, p_{\text{memb}})$ for water and TMAO samples separately using

$$(\mathbf{S}, \mathbf{SV}, \mathbf{L}) = \text{SVD}(\mathbf{Data}), \quad (2)$$

where SVD describes a singular value decomposition of the array data that contains the individual measurements as row vectors.⁵ For our set-up the column vectors of the orthonormal matrix \mathbf{L} contain the spectroscopic information. The columns of the orthonormal matrix \mathbf{S} contain information of the spectral variation and the cell thickness change with increasing pressure. \mathbf{SV} is a diagonal matrix with the singular values that represent the weight of the individual components. Singular value decomposition sorts the data according to their variance. We aim to separate physically meaningful spectral information from the experimentally observed pressure dependency. Precondition of the analysis is that the variance at each frequency component is similar over the full spectral range under consideration. Due to the strong high-frequency absorption for water and TMAO starting at 360 cm^{-1} in our setup, this requirement is not fulfilled. Therefore, we modified our approach and introduced a filtering function of the form

$$F(\nu, \nu_m, \Delta\nu) = \frac{1}{e^{\frac{\nu - \nu_m}{\Delta\nu}} + 1} \quad (3)$$

which was applied to each spectral data set before performing the principal component analysis. The function varies between 1 for $\nu \ll \nu_m$ and 0 for $\nu \gg \nu_m$ and has the value 0.5 at $\nu = \nu_m$. The parameter $\Delta\nu$ determines the width of the transition from unity to zero. For the data discussed here, we used the empirically determined parameters $\nu_m = 380 \text{ cm}^{-1}$ and $\Delta\nu = 12 \text{ cm}^{-1}$. This allows us to increase the accessible frequency range from 360 cm^{-1} to 420 cm^{-1} , which includes the intramolecular TMAO mode at around 385 cm^{-1} .⁶ In the following, we will refer to a principal component as the product of eigenvector and its corresponding singular value. When the thickness $d(p_{\text{memb}})$ is known, $\Delta\tau$ can be approximated by the N most significant pressure dependent score functions $s_i(p_{\text{memb}})$ and the frequency

dependent principal components $PC_i(\tilde{\nu})$. Taking into account that we used $F(\nu, \nu_m, \Delta\nu)\Delta\tau$ as input for the following PCAs, $\Delta\tau$ is given by

$$\begin{aligned}\Delta\tau &\approx \frac{1}{F(\nu, \nu_m, \Delta\nu)} \sum_{i=1}^N s_i(p_{\text{memb}}) PC_i(\tilde{\nu}) \\ &= \sum_{i=1}^N s_i(p_{\text{memb}}) \widetilde{PC}_i(\tilde{\nu})\end{aligned}\quad (4)$$

where we defined $\widetilde{PC}_i(\tilde{\nu}) = \frac{PC_i(\tilde{\nu})}{F(\nu, \nu_m, \Delta\nu)}$ to remove the filtering effect. According to equation 1, the pressure dependent score function $s_i(p_{\text{memb}})$ contains information of both, the thickness changes and the spectroscopic changes and can be written in the form :

$$s_i(p_{\text{memb}}) = d(p_{\text{memb}})f_{\alpha,i}(p_{\text{memb}}) - d(0)f_{\alpha,i}(0)\quad (5)$$

If $d(p_{\text{memb}})$ is known from independent *ex-situ* measurements $\Delta\tau$ can be written as:

$$\Delta\tau = d(p_{\text{memb}}) \sum_{i=1}^N f_{\alpha,i}(p_{\text{memb}}) \widetilde{PC}_i(\tilde{\nu}) - d(0) \sum_{i=1}^N f_{\alpha,i}(0) \widetilde{PC}_i(\tilde{\nu})\quad (6)$$

In this expression, the absorption coefficients of bulk water and the solution $\alpha_{\text{bulk}}(\tilde{\nu}, p_{\text{memb}})$ and $\alpha_{\text{sol}}(\tilde{\nu}, p_{\text{memb}})$, respectively, are given as a sum of a small number of principal components. As example, we obtain

$$\alpha_{\text{sol}}(\tilde{\nu}, p_{\text{memb}}) = \sum_{i=1}^N f_{\alpha,i}(p_{\text{memb}}) \widetilde{PC}_i(\tilde{\nu})\quad (7)$$

with pressure dependent scaling functions $f_{\alpha,i}(p_{\text{memb}})$. To ensure that this approximation holds for both TMAO and water, scaled ambient pressure 1.5 M TMAO solution and water optical thicknesses were added to the TMAO and water data sets, respectively. These data correspond to spacer thicknesses of 0 to 10 μm with 0.5 μm step size. This grants us to receive reference weights $f_{\alpha,i}(0)$ that allow us to express the reference water and TMAO

spectra at ambient pressure as function of principle components $\widetilde{PC}_i(\tilde{\nu})$.

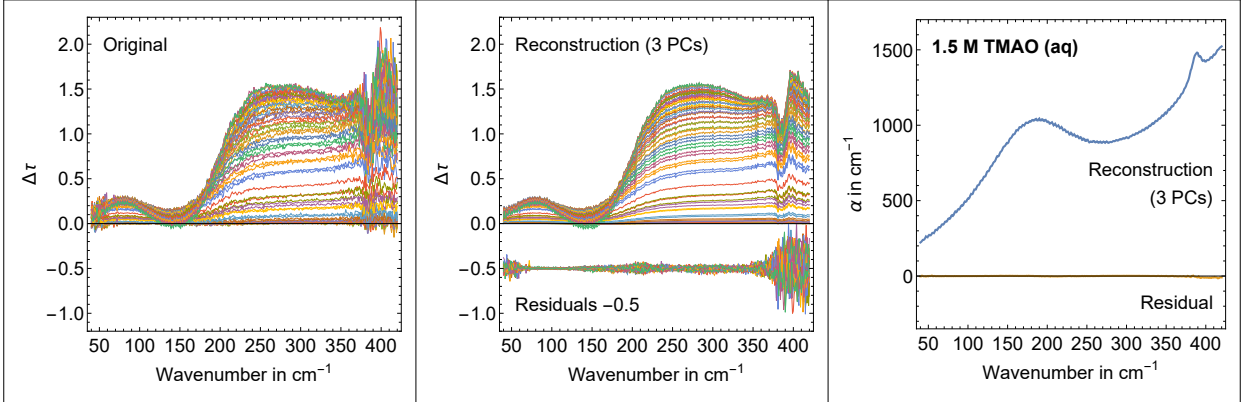


Figure 2: Comparison of the original measurements of aqueous 1.5 M TMAO solutions (left) and the reconstruction (middle) using the three most significant principal components. The residuals between original and reconstructed measurements are shown with an offset of $\Delta\tau = -0.5$. Right: 1.5 M TMAO absorption (blue) at ambient condition as reconstructed from the three most significant principal components. The residual is shown in yellow.

Figure 2 shows the comparison between the original spectra of 1.5 M TMAO solutions and the reconstructed spectra as a result of the PCA. We see that the first three principal components are sufficient to reproduce the observed spectral changes. The residuals are due to systematic and statistical measurement errors (see Figure 2). Figure 3 shows the major principal components of our analysis, together with the pressure dependency of the corresponding scores for two independent measurement series.

Global Analysis of Spectral and Thickness Changes

A systematic error is introduced by the pressure transducer function that connects the applied membrane pressure, p_{memb} (0–18 bar), to the internal sample pressure, p_{sample} (0–12 kbar). This error varies from measurement to measurement, depending on the individual spacer. In general, the pressure transducer function shows two different regimes: the low pressure regime, where the slope $\frac{dp_{\text{sample}}}{dp_{\text{memb}}}$ is small (or almost zero) and the high pressure region, where $\frac{dp_{\text{sample}}}{dp_{\text{memb}}}$ is large (see Figure 2). To minimize the influence of systematic errors, we carried out a global fit of the distinct data sets (pressure calibration, thickness calibra-

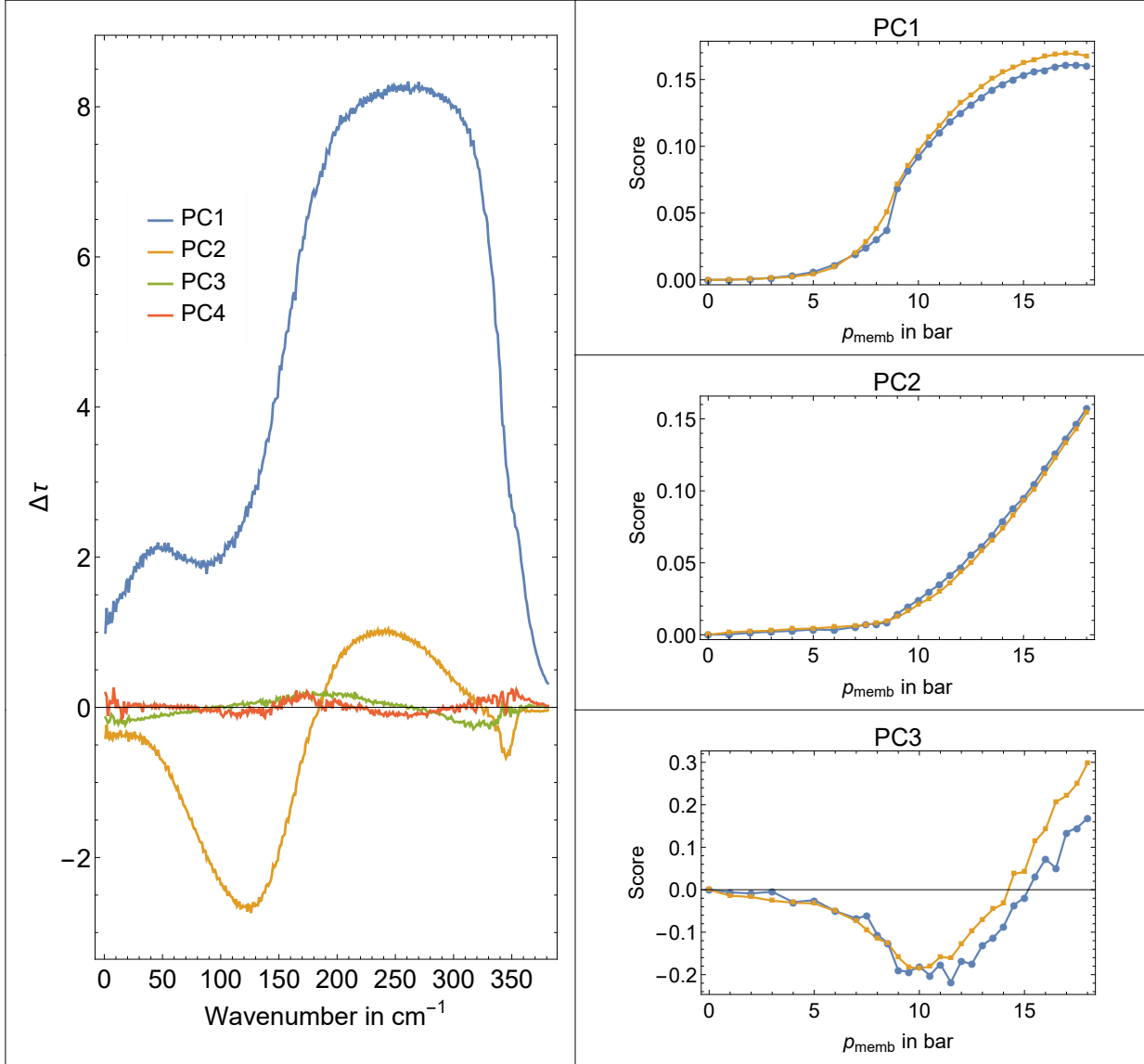


Figure 3: Principal component analysis of the measurement series of the $\Delta\tau$ of 1.5 M TMAO solutions. Left: the dominant four principal components. Right: Scores for the three principal components of single measurements (orange and blue) used for spectroscopic reconstruction as function of p_{memb} . The fourth principle component showed no clear pressure dependence but rather noise.

tion and three principal component scores of the optical depth measurements of pure water and the 1.5 M TMAO solution, respectively) to determine the internal sample pressure, the sample thickness and the spectral changes as a function of the external variable membrane pressure (p_{memb}). To be physically meaningful, we required all fitting functions to be continuous and differentiable as a function of membrane pressure. Such a continuous behavior

is supported by our accompanying theoretical work.

Input data of our global analysis were the center frequencies of the α -quartz peak at 264 cm^{-1} ,^{1,2} the layer thickness as determined by the independent measurements, and the scores of the first three principal components of bulk water (all from our previous measurements described by Vondracek *et al.*²) as well as the scores of the first three principal components of the 1.5 M TMAO solution multiplied by their corresponding principal values. The weights of the frequency and thickness measurements were obtained as $w_i = \frac{1}{\sigma_{0.95}^2}$ where $\sigma_{0.95}$ is the uncertainty of a single measurement point at a 95% confidence level. All other weights were set to unity.

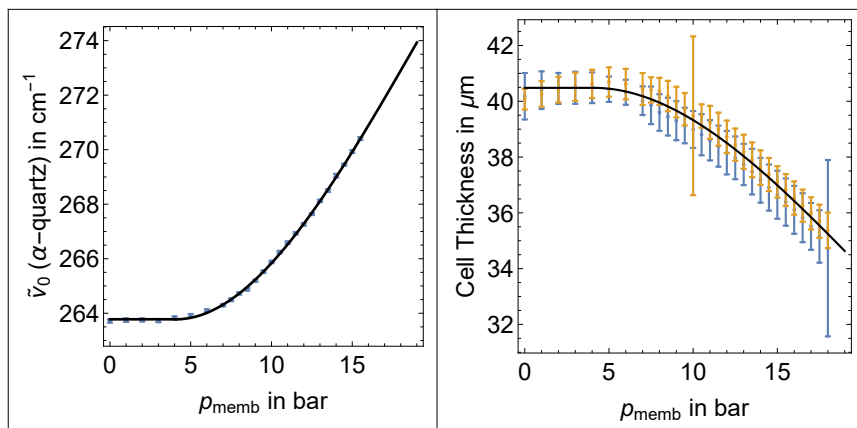


Figure 4: Comparison of the experimental data and the fit of (left): Pressure calibration measurement using α -quartz; (right): Results of two independent thickness measurements (blue and orange).

The results of a weighted global fit of the measurements and scores are shown in Figures 4, 5 and 6. Since all experiments show two regimes with small and large changes of the properties when p_{memb} is changed, we used in all cases stepwise, continuously differentiable functions to describe the experimental data. The regime below the crossover membrane pressure p_{co} at which the sample pressure builds up (i.e. ~ 4.1 bar) is prone to systematic errors. Therefore, we applied the following procedure, which yields physically reasonable results and avoids overfitting: For all cases, the model function was assumed to be constant up to p_{co} . p_{co} was considered to be identical for all model functions. For membrane pressures

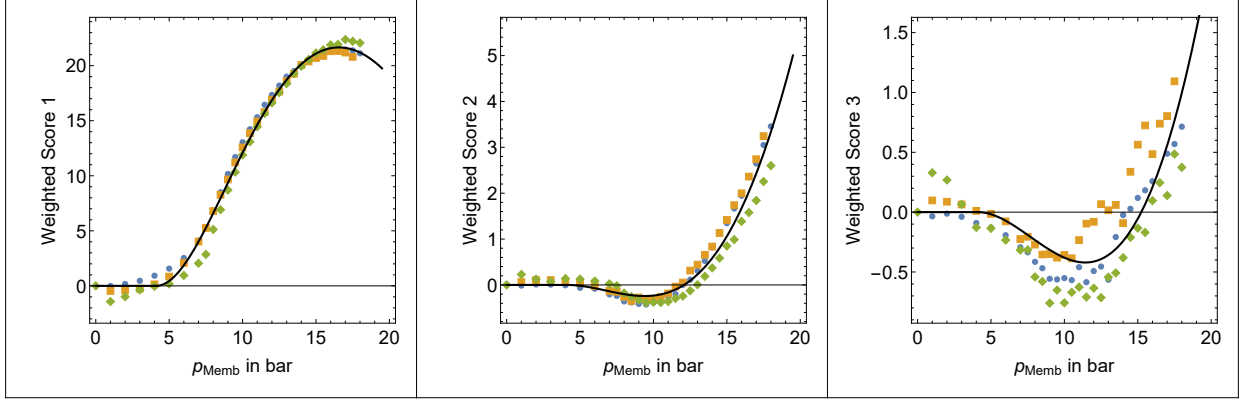


Figure 5: Comparison of the weighted scores of the first three principal components of bulk water and their fit models. Blue, orange and green dots are the independent measurements, the solid black line corresponds to the model.

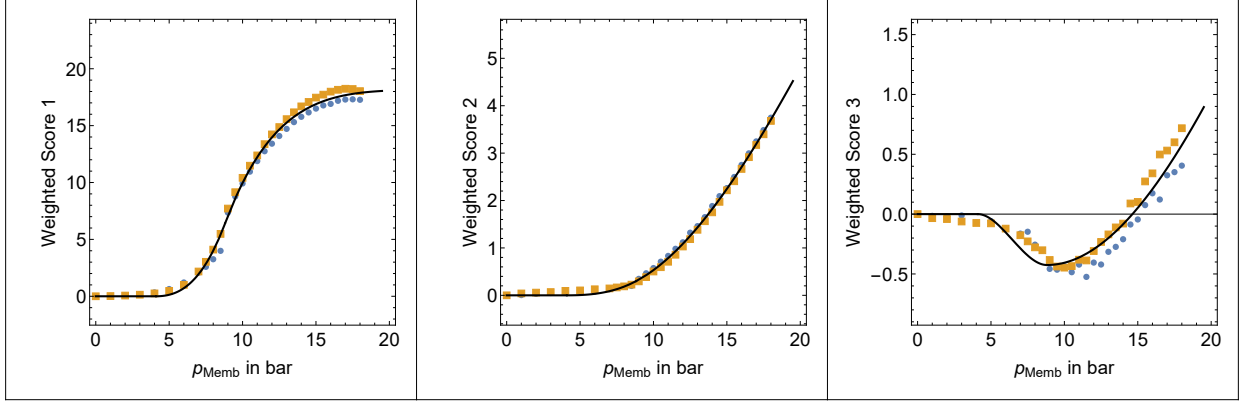


Figure 6: Comparison of the weighted scores of the first three principal components of $\Delta\tau$ of the 1.5 M TMAO solution and their fit models. Blue and orange dots are the independent measurements, the solid black line corresponds to fit model.

above p_{co} , a cubic behavior of $\tilde{\nu}_{264}(p_{memb})$ and $d(p_{memb})$ was assumed (see Figure 4) with the additional constraints that the cubic function approaches the constant value at p_{co} and that its derivative disappears (i.e. vanishing linear term) to ensure continuous differentiability.

Taking advantage of equation 4, we use the following Ansatz for the score functions (Figures 5 and 6):

$$s_i(p_{memb}) = \frac{40\mu m}{d(0)} [d(p_{memb})f_{\alpha,i}(p_{memb}) - d(0)f_{\alpha,i}(0)] \quad (8)$$

This ensures that $s_i(p_{memb}) = 0$ for $p_{memb} = 0$ bar. We introduce a scaling factor $\frac{40\mu m}{d(0)}$ to

rescale the spacer thickness to its nominal value of $40 \mu m$ at ambient pressure. For membrane pressures $p_{\text{memb}} \leq p_{co}$, $f_{\alpha,i}$ was set to the value as obtained from the reconstruction of the water or aqueous TMAO absorption at ambient pressure (see Figure 2) based upon the first three principal components.

Concerning water, we modified the functional description given by Vondracek *et al.*² in the following way: For the first principal component score, $f_{\alpha,1}$ partially reflects the liquid's density change. To ensure continuous differentiability, we found empirically that the functional form

$$\begin{aligned}
 f_{\alpha,1}(p_{\text{memb}}) &= a_{1,0} + \Delta f_{\alpha,1}(p_{\text{memb}}) & (9) \\
 &= a_{1,0} \\
 &\quad + a_{1,1} \left(\frac{1}{e^{p_{\text{memb}}^k} + 1} - \frac{1}{e^{p_{co}^k} + 1} + \frac{k(p_{\text{memb}} - p_{co})e^{p_{co}^k}}{(e^{p_{co}^k} + 1)^2} \right) \\
 &\quad + a_{1,2}(p_{\text{memb}} - p_{co})^2
 \end{aligned}$$

describes the observed changes well for $p_{\text{memb}} > p_{co}$ with a minimum number of parameters. For the second and third principal component of water we chose a cubic approximation with no linear term of $f_{\alpha,i}$ for pressures $p_{\text{memb}} > p_{co}$. In general, the model function matches the measurement very well, as shown in Figure 5. Small systematic deviations can still be found in the membrane pressure range $0 \leq p_{\text{memb}}$ in bar ≤ 6 , which corresponds to a sample pressure range ≤ 1 kbar. For the TMAO solution, the stepwise function consists of three parts (see Figure 6). This is necessary to capture the different pressure behavior of the first and second score functions for TMAO solutions. Again, the low pressure ($p_{\text{memb}} < 4.1$ bar) part is assumed to be constant. The second part in the membrane pressure range 4.1–8.8 bar can be described by cubic functions without a linear term for all three scores. The cubic form is also used to describe the second and third scores in the pressure range above 8.8 bar. The cubic parameters have been chosen such that the boundary condition for continuous differentiability is fulfilled. Again in the first score, the water density becomes essential, but

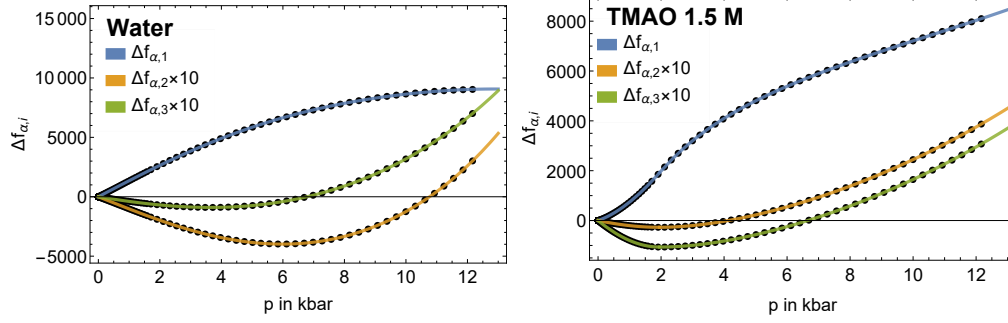


Figure 7: $\Delta f_{\alpha,i}$ for water (left) and TMAO (right) and the corresponding polynomial fits as function of sample pressure.

now only at membrane pressures above 8.8 bar. The model function

$$\begin{aligned}
 f_{\alpha,1}(p_{\text{memb}}) &= a_{1,0} + a_{1,1}(p_T - p_{co})^2 + a_{1,2}(p_T - p_{co})^3 \\
 &+ a_{1,3} \left(\frac{1}{e^{p_{\text{memb}}k} + 1} - \frac{1}{e^{p_Tk} + 1} \right) \\
 &- (p_{\text{memb}} - p_{co}) \left[(p_T - p_{co}) [2a_{1,1} + 3a_{1,2}(p_T - p_{co})] + \frac{a_{1,3}k e^{p_Tk}}{(e^{p_Tk} + 1)^2} \right] \\
 &+ (p_{\text{memb}} - p_{co})^2 \left(2a_{1,1} - 3a_{1,2}p_{co} + 3a_{1,2}p_T + \frac{a_{1,3}k e^{p_Tk}}{(p_T - p_{co})(e^{p_Tk} + 1)^2} \right)
 \end{aligned} \tag{10}$$

is used to describe the observed changes with a minimum number of parameters. Here, p_{co} is the same as for water and $p_T = 8.8$ bar membrane pressure describes the second pressure step where the physical change of the TMAO solution is taking place. It corresponds to a solution pressure of $p_{\text{sample}} = 1.95$ kbar. Please note that all other parameters are different for TMAO and water. The result of the global fit for the TMAO scores is seen in Figure 6. Since our global model contains p_{sample} , d_{sample} as well as $f_{\alpha,i}$, ($i = 1-3$) as function of membrane pressure (p_{Memb}) for water and 1.5 M TMAO, respectively, we can directly relate $f_{\alpha,i}$ to p_{sample} . For water, $\Delta f_{\alpha,i}$, ($i = 1-3$) can be well described by polynomials of degree five as a function of sample pressure. In the case of TMAO, the pressure range below 1.95 kbar sample pressure can be described by third-order polynomials, while for higher sample pressures sixth-order polynomials were used. In the full model we used the additional constraint of continuous differentiability. Based upon this description, we were able to determine α_{TMAO}

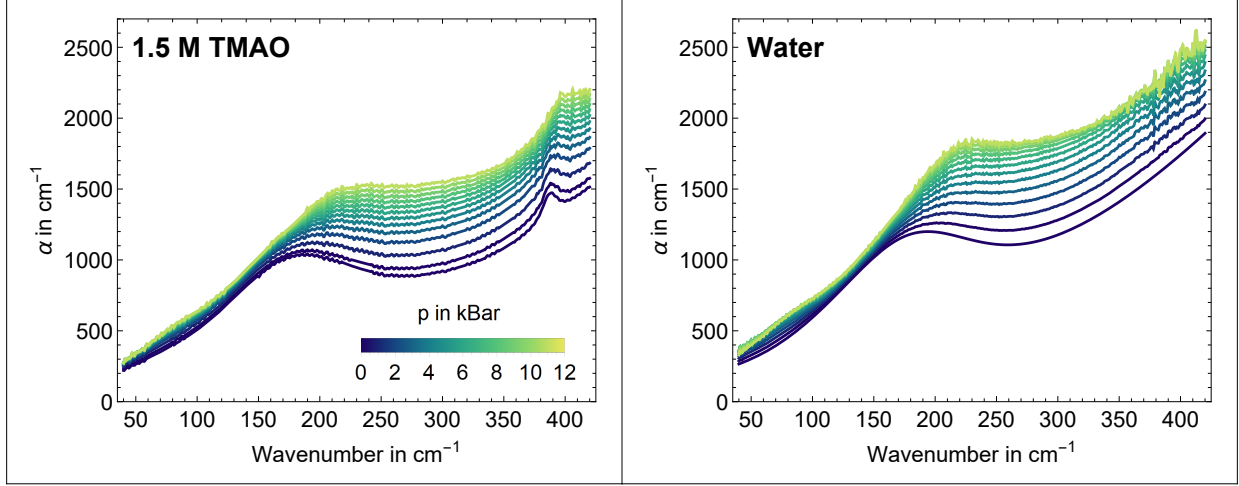


Figure 8: Absorption of 1.5 M TMAO (left) and water (right) as a function of sample pressure.

and α_{bulk} as function of sample pressure p_{sample} (see Figure 8).

Pressure-dependent Apparent Molar Volume of TMAO in Water

To obtain molar properties, we have to correct the data for pure pressure-dependent density changes. Therefore, we use the pressure and temperature independent molality b_{sol} and its related solute mole fraction x :

$$b_{\text{sol}} = \frac{n_{\text{solute}}}{m_{\text{water}}} \quad (11)$$

$$x = \frac{n_{\text{solute}}}{n_{\text{solute}} + n_{\text{water}}} \quad (12)$$

with n_{solute} , n_{water} and m_{water} marking the number of TMAO molecules, the number of water molecules and the mass of 1000 g for the sample, respectively. As a precise and sensitive measure of the volume effect of the dissolved solute, we use the apparent molar volume

$$V_{\phi} = \frac{M_{\text{TMAO}}}{\rho_{\text{sol}}(p, T)} - \frac{\rho_{\text{sol}}(p, T) - \rho_{\text{water}}(p, T)}{\rho_{\text{sol}}(p, T) \cdot \rho_{\text{water}}(p, T) \cdot b_{\text{sol}}} \quad (13)$$

with the molar mass of the solute TMAO: M_{TMAO} , the pressure and temperature-dependent density of the given solution $\rho_{\text{sol}}(p)$ and the pressure-dependent density of water $\rho_{\text{water}}(p)$ as

the solvent.

Pressure, temperature and composition dependent density data are available from Makarov *et al.*⁷ ($p \leq 1$ kbar, $298.15 \text{ K} \leq T \leq 323.15 \text{ K}$, $0.0875 \text{ mol kg}^{-1} \leq b \leq 4.3251 \text{ mol kg}^{-1}$) and from Knierbein *et al.*⁸ ($T = 298.15 \text{ K}$) who investigated a $2.348 \text{ mol kg}^{-1}$ solution in the pressure range from ambient to 5 kbar using neutron scattering. Since none of the data sets match exactly our measurement conditions, we modeled $V_\phi(p, x, \theta)$ as a quadratic function of pressure p (in bar), mole fraction x and temperature θ (relative to 25°C). The model is continuously differentiable and consists of two parts. In the pressure range below the transition pressure p_0 , the model has the form

$$\begin{aligned}
V_\phi(p, x, \theta) = & c000 + c001(\theta - 25.) + c002(\theta - 25.)^2 \\
& + [c010 + c011(\theta - 25.) + c012(\theta - 25.)^2] x + c020 x^2 \\
& + [c100 + c101(\theta - 25.) + c102(\theta - 25.)^2 \\
& + \{c110 + c111(\theta - 25.) + c112(\theta - 25.)^2 + c120 x\} x] p \\
& + [c100H + 2 \times c200H p000 - c100 - c101(\theta - 25.) - c102(\theta - 25.)^2 \\
& - \{c110 + c111(\theta - 25.) + c112(\theta - 25.)^2\} x - c120 x^2] \frac{p^2}{2 \times p0}.
\end{aligned} \tag{14}$$

Above p_0 , the model has the form

$$\begin{aligned}
V_\phi(p, x, \theta) = & \frac{1}{2}[2 c000 + 2 c001(\theta - 25.) + 2 c002(\theta - 25.)^2 \\
& + 2 c010 x + 2 c011(\theta - 25.)x + 2 c012(\theta - 25.)^2x + 2 c020x^2 \\
& + c100 p0 + c101(\theta - 25.)p0 + c102(\theta - 25.)^2p0 \\
& + c110p0x + c111(\theta - 25.)p0x + c112(\theta - 25.)^2p0x + c120p0 x^2 \\
& + 2(p - p0) \{c100H + 2 c200H p0\} + c100H p0 + 2 c200H p0^2]
\end{aligned} \tag{15}$$

The coefficients c reflect the internal pressure p , mole fraction x and temperature θ : $px\theta$. The coefficients are labeled according to their polynomial degree, i.e. 0 is a constant, 1 a

linear and 2 a quadratic term. Any coefficients with an H are adapted to the high-pressure part. The fit parameters of $V_\phi(p, x, \theta)$ are summarized in Table 1. In the following chapter, we use the result of the fit for V_ϕ . This results are visualized at Figure 9 as well as measured data of Knierbein *et al.*⁸ and Makarov *et al.*⁷ at close conditions to our own measurements for comparison.

Table 1: Parameters for the $V_\phi(p, x, \theta)$ (See equation 15 and 16) with standard error

parameter	value	standard error
$c100H$	$-2.276 \cdot 10^{-3}$	$3.04 \cdot 10^{-4}$
$c200H$	0	0
$c000$	73.2294	$1.41 \cdot 10^{-2}$
$c001$	$2.6111 \cdot 10^{-2}$	$9.35 \cdot 10^{-4}$
$c002$	0	0
$c010$	-26.732	$2.55 \cdot 10^{-1}$
$c011$	$3.625 \cdot 10^{-1}$	$1.59 \cdot 10^{-2}$
$c012$	$-3.871 \cdot 10^{-3}$	$3.35 \cdot 10^{-4}$
$c020$	0	0
$c100$	$1.0497 \cdot 10^{-3}$	$5.23 \cdot 10^{-5}$
$c101$	$-2.257 \cdot 10^{-5}$	$1.94 \cdot 10^{-6}$
$c102$	$3.948 \cdot 10^{-7}$	$3.91 \cdot 10^{-8}$
$c110$	$-1.053 \cdot 10^{-2}$	$1.72 \cdot 10^{-3}$
$c111$	$-2.045 \cdot 10^{-4}$	$3.21 \cdot 10^{-5}$
$c112$	0	0
$c120$	$8.53 \cdot 10^{-2}$	$1.68 \cdot 10^{-2}$
$p0$	3385	400

Pressure-dependent Average Extinction

The effective absorption of a solution is defined as:^{2,9}

$$\alpha_{\text{sol}}^{\text{eff}} = \alpha_{\text{sol}} - \frac{1}{V_{0,\text{bulk}}} (1 - c_s V_\phi) \epsilon_{\text{bulk}} = \alpha_{\text{sol}} - (1 - c_s V_\phi) \alpha_{\text{bulk}} \quad (16)$$

with α_{sol} as absorption of the solution, V_0 as molar volume of the bulk solvent, c_s as solute concentration and ϵ_{bulk} and α_{bulk} as bulk molar extinction coefficient and bulk absorption coefficient, respectively. Here, V_ϕ is the apparent molar volume of the solute, which is defined

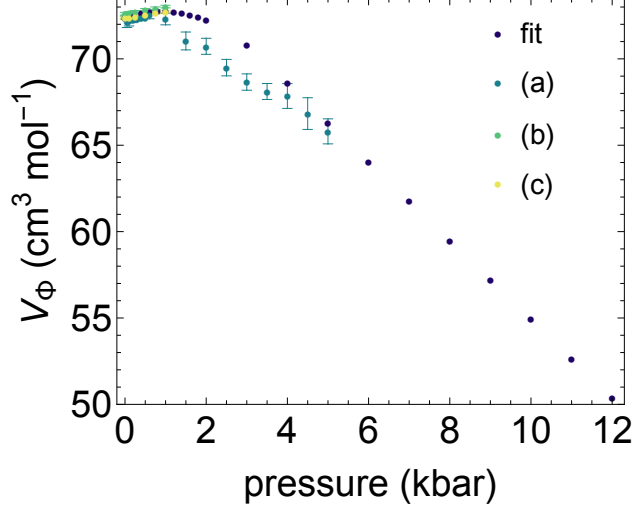


Figure 9: fit: Apparent molar volume $V_{\Phi}(p, 0.029, 23^{\circ}C)$ used for our data analysis from the fit; (a) x-ray scattering results from Knierbein *et al.*⁸ of $V_{\Phi}(p, 0.041, 25^{\circ}C)$; (b) U-tube densitometer results of Makarov *et al.*⁷ of $V_{\Phi}(p, 0.024, 25^{\circ}C)$ and c) of $V_{\Phi}(p, 0.033, 25^{\circ}C)$

from:

$$c_s V_{\phi} + c_w V_0 = 1 \quad (17)$$

where c_w is the water concentration in the solution. Since the solute and solvent concentrations change with changing pressure - while mole fraction remains constant - we replace the concentration by the mole fraction x using

$$c_s = \frac{x}{(1-x)V_0 + xV_{\phi}}. \quad (18)$$

This yields

$$\alpha_{\text{sol}}^{\text{eff}} = \alpha_{\text{sol}} - \frac{(1-x)V_0\alpha_{\text{bulk}}}{(1-x)V_0 + xV_{\phi}}. \quad (19)$$

V_0 and V_{ϕ} can be expressed in terms of the measured densities ρ_{bulk} and ρ_{sol} of the bulk solvent and the solution, respectively. With increasing internal pressure, the density of the probed volume is increased, leading to more water molecules inside the volume. To account for this effect, we consider the effective molar extinction coefficient $\epsilon_{\text{sol}}^{\text{eff}} = \frac{\alpha_{\text{sol}}^{\text{eff}}}{c_s}$ of a solution as function of mol fraction, densities and absorption coefficients of bulk solvent and solution,

respectively. Using the equations 18 and 19, we can determine

$$\epsilon_{sol}^{\text{eff}} = \Phi_V \alpha_{sol} + \frac{M_w (1-x)}{\rho_{\text{bulk}} x} (\alpha_{sol} - \alpha_{\text{bulk}}), \quad (20)$$

where we have made use of the fact that the molar volume of the bulk solvent is related to the density via

$$V_0 = \frac{M_w}{\rho_{\text{bulk}}} \quad (21)$$

with M_w being the molar mass of water.

Pressure-dependent Fit of the Average Extinction

We have shown before, that in general $\epsilon_{\text{sol}}^{\text{eff}}$ can be well described for several compounds by the superposition of a negatively scaled bulk water extinction coefficient ϵ_{bulk} and a positive combination of damped harmonic oscillators:^{5,9}

$$\epsilon_{\text{TMAO}}^{\text{eff}}(\nu, p) = -N_{\text{hyd}} \epsilon_{\text{bulk}}(\nu, p) + \sum_{i=1}^N f_i(\nu, \nu_{D,i}, A_i, \Delta_i). \quad (22)$$

Here, the scaling factor N_{hyd} accounts for the number of water molecules per TMAO molecule that are spectroscopically different from bulk water at the same conditions. The damped harmonic oscillator line shape $f_i(\nu, \nu_{D,i}, A_i, \Delta_i)$ has the form

$$f_i(\nu, \nu_{D,i}, A_0, \Delta_i) = \frac{A_i \nu^2 \Delta_i^2}{4\pi^3 [(\nu_{D,i}^2 + (\frac{\Delta_i}{2\pi})^2 - \nu^2)^2 + 4 (\frac{\Delta_i}{2\pi})^2 \nu^2]} \quad (23)$$

where A_i is the amplitude, Δ_i the width, and $\nu_{D,i}$ the apparent center frequency of the damped oscillator. The unperturbed center frequency $\nu_{0,i}$ of the undamped oscillator is given by

$$\nu_{0,i} = \sqrt{\nu_{D,i}^2 + \left(\frac{\Delta_i}{2\pi}\right)^2} \quad (24)$$

For details, see Refs. 3,9. Each spectrum of $\epsilon_{\text{TMAO}}^{\text{eff}}(\nu, p)$ is dissected into a sum of five damped harmonic oscillators (equation 23) and N_{hyd} (Figure 10). To ensure stable fits over the complete pressure and wavenumber range, we constrain the $\nu_{D,i}$ of the low-frequency oscillator to 0 cm^{-1} .¹⁰ The same width for the oscillators at 283 cm^{-1} and 446 cm^{-1} has been assumed. The center frequencies $\nu_{D,i}$, the amplitude A_i and the width Δ_i of the five oscillators (f_I - f_V) of the spectral dissection of $\epsilon_{\text{TMAO}}^{\text{eff}}(\nu, p)$ at different pressures are shown in the following Figures 11 - 15. Also, the results for N_{Hyd} are shown in Figure 16. Since subtle changes in the observed line shape can be accounted for in the fit by simultaneous increase of N_{Hyd} and a similar increase in the apparent amplitudes of the oscillators, we normalize the amplitudes by N_{Hyd} (see Figure 17) except the one of the intramolecular CNC bending mode at 387.2 cm^{-1} (at ambient conditions) = (IV). Details are discussed in the main text.

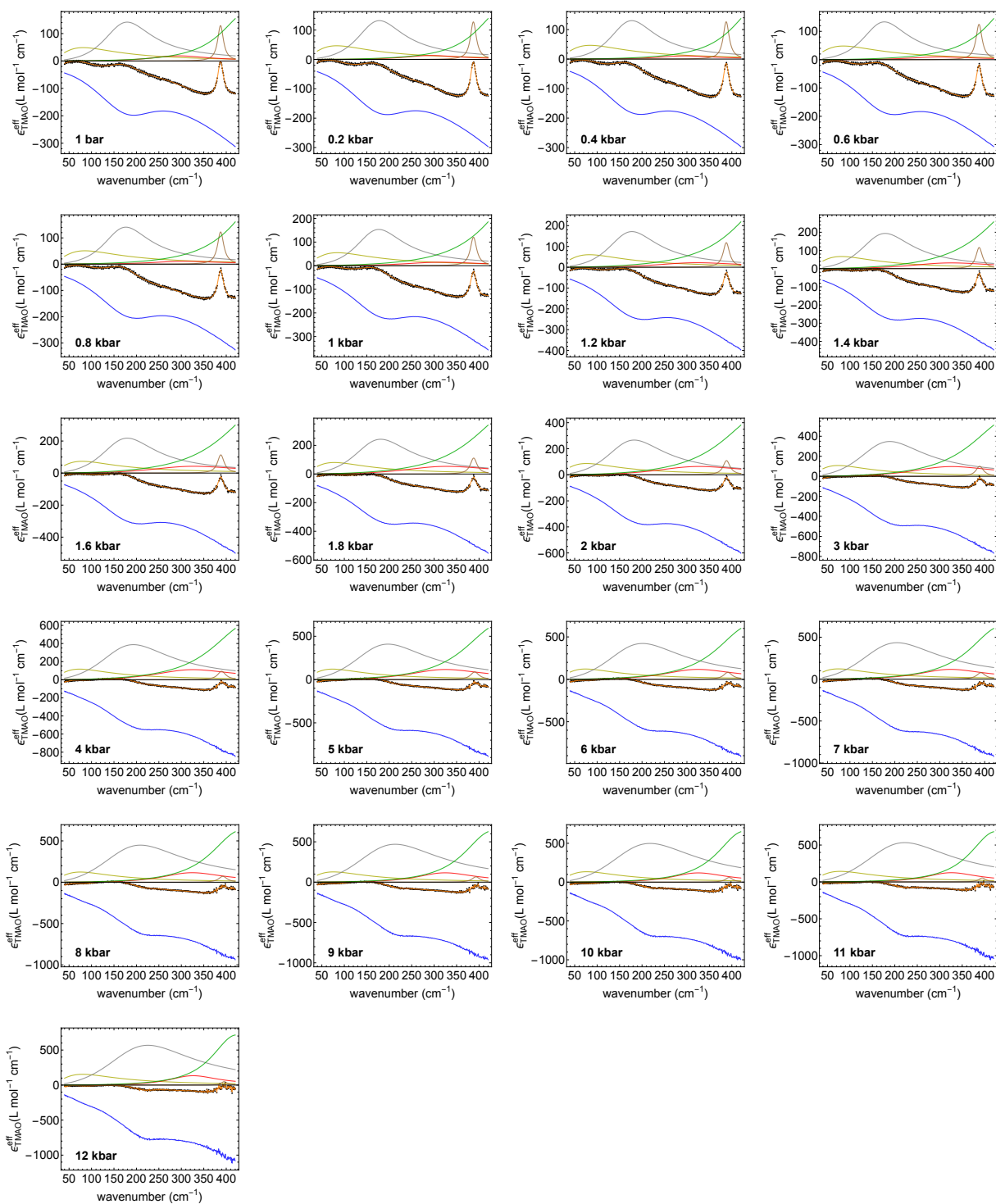


Figure 10: Dissection of aqueous TMAO spectra at different pressures. The dotted black curve corresponds to the experimental spectrum, the orange line to the fit. The blue line is $N_{\text{Hyd}}\epsilon_{\text{bulk}}$. The dark yellow, gray, bright red, brown and the green solid lines are the fitted damped harmonic oscillators

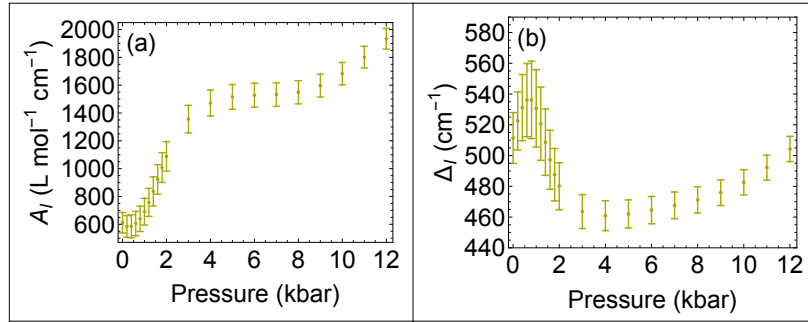


Figure 11: (a) Amplitude A_I and (b) width Δ_I of the oscillator f_I with the fixed center frequencies $\nu_{D,I} = 0 \text{ cm}^{-1}$.

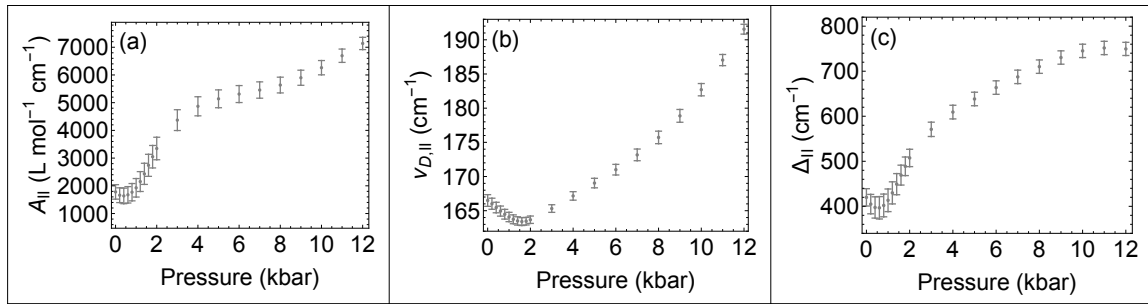


Figure 12: (a) A_{II} , (b) $\nu_{D,II}$ and (c) Δ_{II} (right panel) of f_{II} with $\nu_{D,II} = 165.5 \text{ cm}^{-1}$ (at ambient conditions)

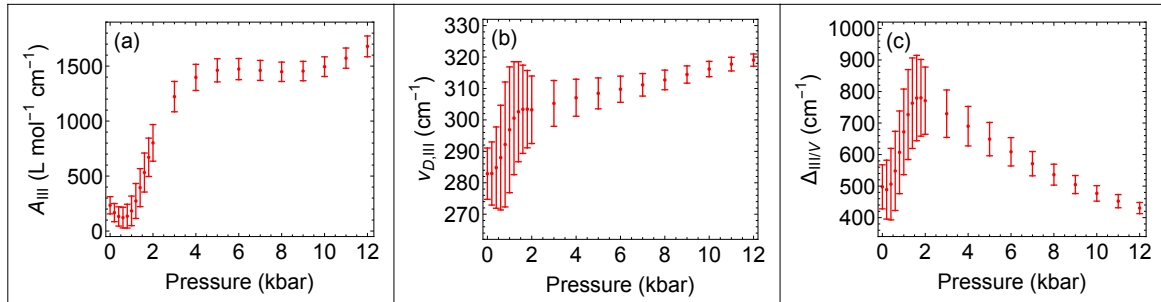


Figure 13: (a) A_{III} and (b) $\nu_{D,III}$ of f_{III} with $\nu_D = 283 \text{ cm}^{-1}$ (at ambient conditions). (c) $\Delta_{III/V}$ of f_{III}/f_V .

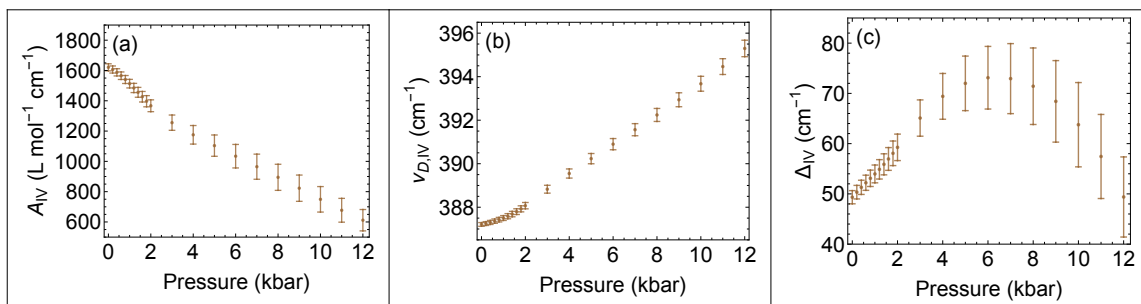


Figure 14: (a) A_{IV} , (b) $\nu_{D,IV}$ and (c) Δ_{IV} of f_{IV} with $\nu_{D,IV} = 387.2 \text{ cm}^{-1}$ (at ambient conditions).

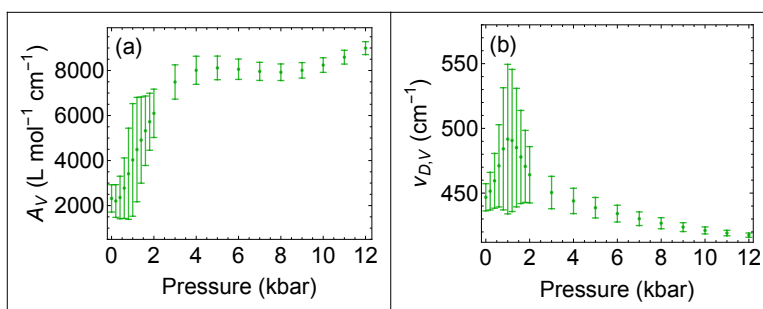


Figure 15: (a) A_V and (b) $\nu_{D,V}$ of f_V with $\nu_{D,V} = 446 \text{ cm}^{-1}$ (at ambient conditions).

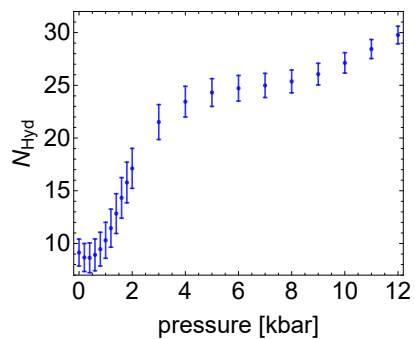


Figure 16: Number of hydration water N_{Hyd} as function of pressure.

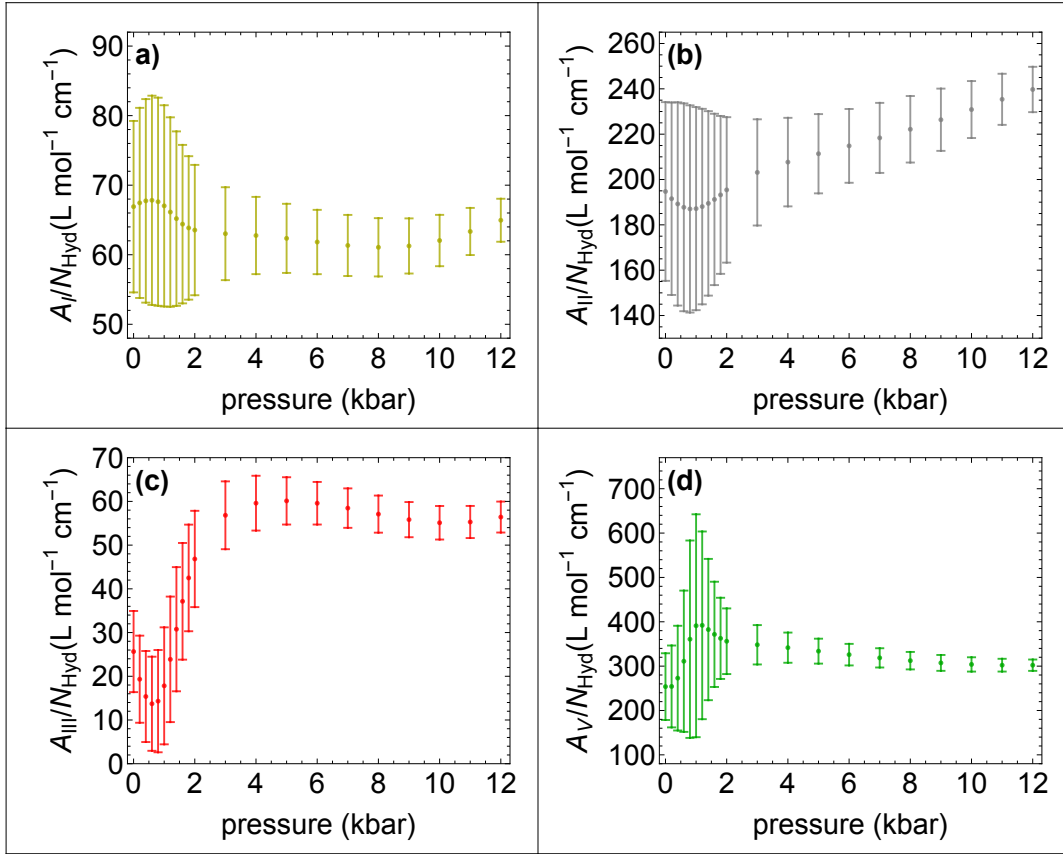


Figure 17: A_i/N_{Hyd} of oscillators (a) f_I , (b) f_{II} , (c) f_{III} and (d) f_V with pressure.

Force Field Molecular Dynamics

Details of the simulation as well as the force field parameters for the TMAO model, which uses different charges for each pressure, are reported in Ref. 11.

Hydrogen-bonding of TMAO

For this analysis, we determine how many water molecules are H-bonded to the oxygen site of TMAO. We use throughout the present study the geometric H-bond criterion as parameterized previously in Ref. 12: A H-bond between TMAO and a water molecule exists if

$$r_{\text{HW}\dots\text{OT}} < -1.71 \text{ \AA} \cdot \cos(\theta_{\text{OW-HW}\dots\text{OT}}) + 1.37 \text{ \AA}, \quad (25)$$

where HW and OW refer to water hydrogen and oxygen atoms and OT to the TMAO oxygen atom and r denotes the respective distance and θ stands for the corresponding angle.

Hydration Number of TMAO

From the simulations TMAO in water, the average number of first shell hydration water molecules is calculated as a function of pressure. The total hydration number is the sum of two contributions, the first one is the number of water molecules that solvate the TMAO oxygen. In Figure 18 the radial distribution function of water oxygen around TMAO oxygen, $g(r_{\text{OW-OT}})$, with and without water-TMAO H-bonds is shown for pressures of 1 bar and 10 kbar. Since essentially all water molecules in the first hydration shell around TMAO oxygen are H-bonded, the first shell hydration number around TMAO oxygen is the average number of H-bonded water molecules which is shown in Figure 19.

The second contribution to the total hydration number is given by the average number of water molecules within the first solvation shell around the three methyl groups of TMAO. To determine the size of this hydration layer, we calculate here the proximal radial distribution

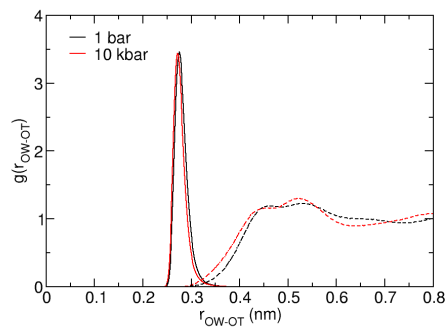


Figure 18: Radial distribution of water oxygen around TMAO oxygen for H-bonded (full lines) and non-hydrogen bonded (dashed lines) molecules.

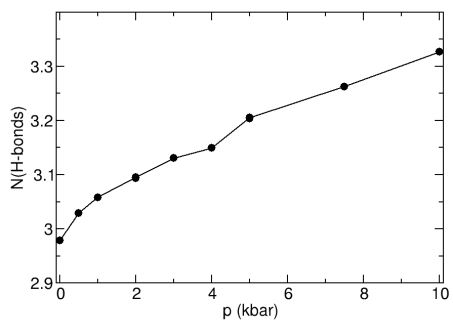


Figure 19: Average number of water-TMAO H-bonds per TMAO molecule.

function between the water oxygen atoms and the TMAO carbon atoms, i.e. the radial distribution calculated by using the shortest distance between water oxygen and the three TMAO carbon atoms, for all water-TMAO pairs that are not H-bonded to the O-site of TMAO, yielding $g^p(r_{OW-CT})$ as depicted in Figure 20. Due to the compression of the first hydration shell with pressure, the first minimum of the proximal distribution decreases from about 4.75 Å at 1 bar to 4.51 Å at 10 kbar. The number of hydration water molecules around the three methyl groups is then defined as the number of water molecules with a shortest distance between water oxygen and TMAO carbon that is shorter than the position of the first minimum of this proximal distribution (Figure 21). Finally, the total hydration number (see the main article) according to simulation is the sum of the number of H-bonds and the number of hydration water molecules around the methyl groups as reported in Figures 19

and 21 as a function of pressure.

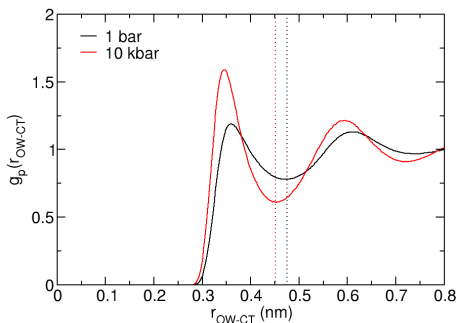


Figure 20: Proximal radial distribution of water oxygen around TMAO carbon atoms for non-hydrogen bonded molecules at 1 bar and 10 kbar. The vertical dotted lines mark the first minima as given in the text.

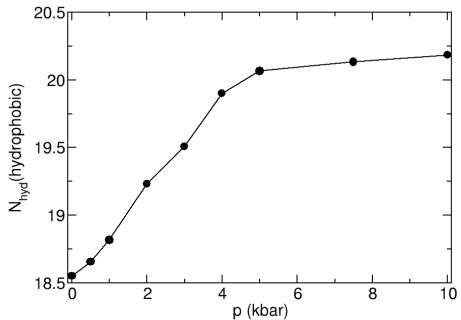


Figure 21: Average number of water molecules within the first shell around the TMAO methyl groups. Only the water molecules without a water-TMAO H-bond are considered as explained in the text.

Assessing Pressure Conditions

In order to estimate the average pressure and its convergence in AIMD simulations carried out at constant volume conditions, we simulated the same TMAO(aq) solutions as in AIMD but using FFMD instead, in particular employing the same densities. These correspond to experimental pressures of the respective solutions at 1 bar and 10 kbar at ambient temperature. The corresponding supercell parameters for one TMAO molecule hosted by

107 H₂O molecules are 14.9382 Å at 1 bar and 13.9223 Å at 10 kbar as determined in earlier AIMD work.¹² We note in passing that following this approach of using experimental equation-of-state information is the *de facto* standard to set up AIMD simulations of aqueous solutions in view of significant involvement in meaningfully carrying out constant pressure AIMD simulations (establishing the NpT ensemble) and, secondly, to statistically converge the stress tensor by sampling (see for instance Sections 3.4.4 and 5.2.3 of Ref.¹³ for general background) despite stress tensor AIMD implementations being widely available including that in the CP2k package¹⁴ that we employ.

In the specific case of the RPBE-D3 functional used here to simulate pure water as well as TMAO(aq) solutions at pressures of 1 bar and 10 kbar at 300 K, it has already been demonstrated that the aforementioned NVT AIMD approach indeed works satisfactorily compared to experiment. For water itself, the radial distribution functions compare favorably to experimental ones, in particular to those available at 10 kbar conditions.¹² Importantly, also the pressure-induced changes of the THz spectrum of bulk water from 1 bar to 10 kbar are described very well with reference to the pressure-dependent experimental spectra.² Specifically for TMAO(aq), our approach has been demonstrated to describe well the intermolecular vibrations of solvated TMAO at ambient conditions compared to experimental THz (far-IR) spectroscopy.¹⁵ At the level of vibrational spectroscopy, it was successful to explain pressure-induced mid-IR frequency shifts of intramolecular TMAO vibrations at 10 kbar relative to 1 bar as detected in high-pressure FT-IR experiments.¹⁶

In order to more explicitly assess the pressure conditions of the TMAO(aq) simulations at 1 bar and 10 kbar using NVT AIMD simulations at 300 K in conjunction with the afore-defined supercell parameters, we applied FFMD simulations. These can very easily sample many nanoseconds to converge the pressure tensor, rather than only averaging it for many picoseconds as in AIMD. This is possible since we previously parameterized a pressure-dependent force field, TMAO-V3-HP(p), to describe TMAO in aqueous solutions all the way from $p = 1$ bar to 10 kbar at 300 K as gauged by both, experimental data as well as

AIMD simulations; we refer to Ref. 11 for background and details. In particular, this tailored force field describes well the thermodynamics of TMAO(aq) solutions at 300 K, in particular the crucial activity coefficient derivative y_{TT} of TMAO in water, as demonstrated earlier¹¹. It also captures the pressure-induced changes in H-bonding of TMAO upon compression from 1 bar to 10 kbar as confirmed by subsequent mid-IR experiments.¹⁶ Overall, these multiple validations support the conclusion that the TMAO-V3-HP(p) force field faithfully describes the properties of aqueous TMAO solutions in close accord with AIMD simulations using the current protocol. Thus, this force-field can be used to converge the pressure tensor within FFMD, allowing us to approximately estimate the intrinsic average pressure in the constant volume AIMD simulations at 300 K.

Essentially the same protocol as explained in the main text has been used to carry out these FFMD simulations at 300 K in the NVT ensemble, but now using a single TMAO in a periodic supercell containing 107 water molecules to represent the system size of the AIMD simulations in conjunction with using the same cubic box lengths of 14.9382 Å / 13.9223 Å at 1 bar / 10 kbar. Due to the small box sizes at the level of FFMD, the cutoffs of the Lennard-Jones potentials and of the real-space part of the Coulomb potential have been set to 0.7 nm / 0.65 nm at 1 bar / 10 kbar.

As one can see from the insets in the respective Figures 22 and 23, the instantaneous pressures (blue lines in the insets) fluctuate enormously, as expected, namely by roughly ± 3 kbar in the two simulations corresponding to 1 bar and 10 kbar conditions. The converged average pressures of about 14 bar and 9.6 kbar, respectively, marked by red horizontal lines have been determined only after extending the FFMD simulations to a duration of 10 ns (not shown). As one can see by monitoring in the main graphs the deviations of the accumulated averages (black lines) from the converged averages (red lines) on the visualized sampling time scale on the order of 100 ps, sampling well beyond the time scale accessible to AIMD simulations is required to meaningfully converge such pressure estimates. But, importantly, it becomes clear that the average pressures determined by our current approximate procedure are close

to the target thermodynamic pressures of TMAO(aq) at 1 bar and 10 kbar. This finding is in full accord with the previously documented^{12,15,16} good agreement of structural and spectroscopic observables of TMAO(aq) solutions at ambient temperature as obtained from our AIMD simulations at 1 bar and 10 kbar when compared to experiments carried out at pressures of 1 bar and 10 kbar.

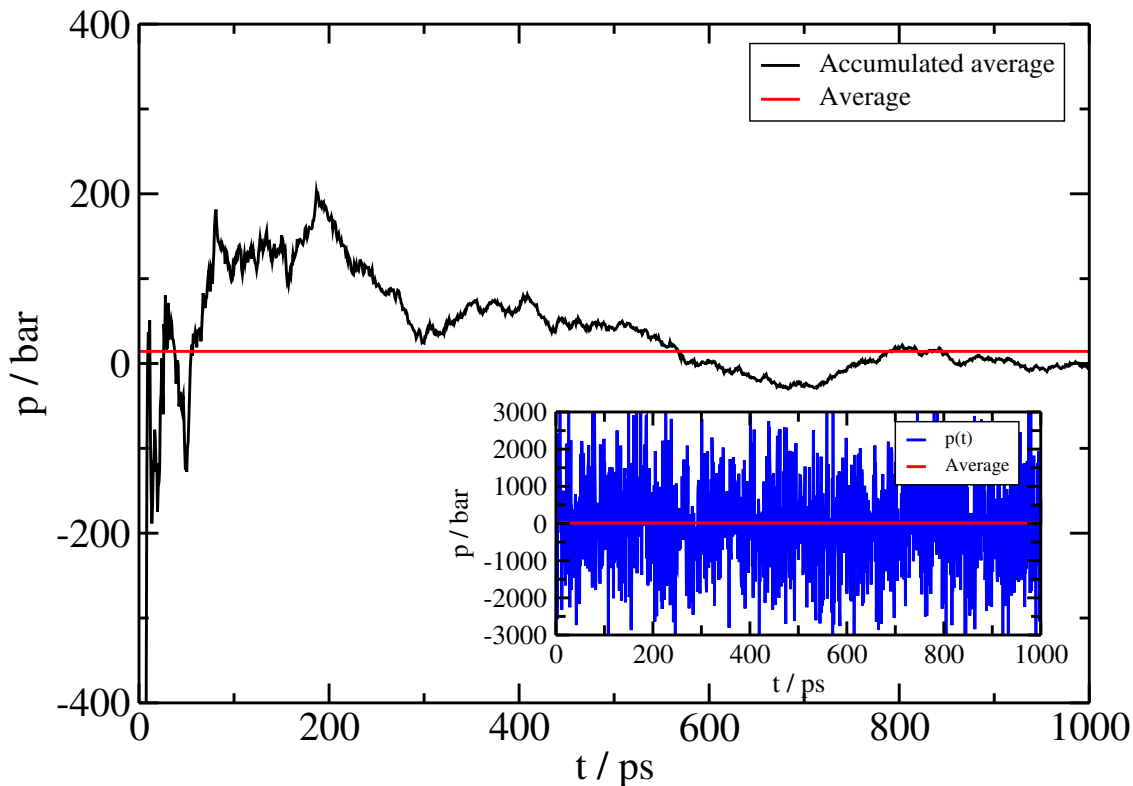


Figure 22: Pressure calculation in the FFMD *NVT* simulation of 1 TMAO solvated by 107 water molecules in a periodic cubic supercell at the experimental density of the solution at 1 bar as used for the AIMD *NVT* simulation at 300 K, see text. The accumulated average (black line) is the average of the instantaneous pressure (blue line in the inset) up to simulation time t . The converged average pressure (14 bar, red lines) has been obtained by extending this simulation up to 10 ns.

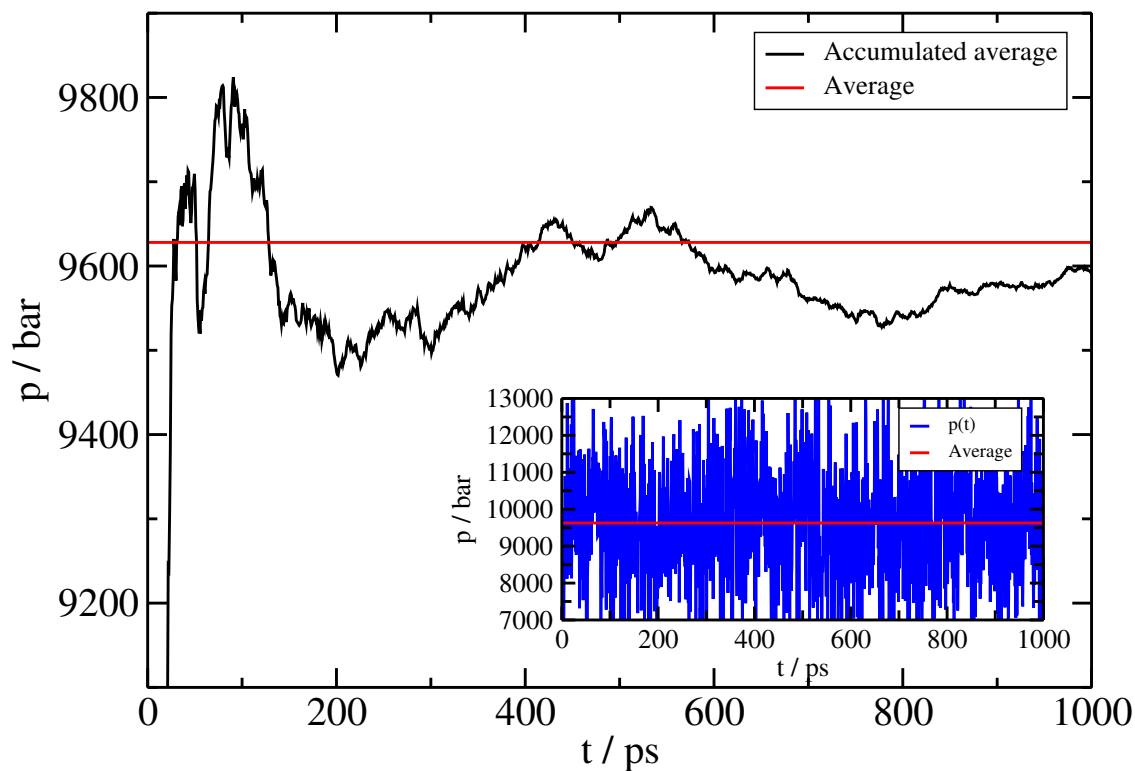


Figure 23: Pressure calculation in the FFMD *NVT* simulation of 1 TMAO solvated by 107 water molecules in a periodic cubic supercell at the experimental density of the solution at 10 kbar as used for the AIMD *NVT* simulation at 300 K, see text. The accumulated average (black line) is the average of the instantaneous pressure (blue line in the inset) up to simulation time t . The converged average pressure (9628 bar, red lines) has been obtained by extending this simulation up to 10 ns.

References

- (1) Knake, L.; Vondracek, H.; Havenith, M. A novel set-up to investigate the low-frequency spectra of aqueous solutions at high hydrostatic pressure. Rev. Sci. Instrum. **2016**, 87, 1–5.
- (2) Vondracek, H.; Imoto, S.; Knake, L.; Schwaab, G.; Marx, D.; Havenith, M. Hydrogen-Bonding in Liquid Water at Multi-Kilobar Pressures. The Journal of Physical Chemistry B **2019**, 0, null, PMID: 31419128.
- (3) Alfarano, S. R.; Vondracek, H.; Sebastiani, F.; Novelli, F.; Hoberg, C.; Kolling, I.; Brubach, J.-B.; Roy, P.; Schwaab, G.; Havenith, M. Does hydrated glycine act as solidification nucleus at multi-kilobar conditions? Biophysical Chemistry **2019**, 253, 106215.
- (4) Voute, A.; Deutsch, M.; Kalinko, A.; Alabarse, F.; Brubach, J.-B.; Capitani, F.; Chappuis, M.; Phuoc, V.; Sopracase, R.; Roy, P. New High-Pressure/Low-Temperature Set-up Available at the AILES Beamline. Vibrational Spectroscopy **2016**, 86.
- (5) Sharma, V.; Böhm, F.; Schwaab, G.; Havenith, M. The low frequency motions of solvated Mn_{ii} and Ni_{ii} ions and their halide complexes. Phys. Chem. Chem. Phys. **2014**, 16, 25101–25110.
- (6) Knake, L.; Schwaab, G.; Kartaschew, K.; Havenith, M. Solvation Dynamics of Trimethylamine N-Oxide in Aqueous Solution Probed by Terahertz Spectroscopy. The Journal of Physical Chemistry B **2015**, 119, 13842–13851, PMID: 26214376.
- (7) Makarov, D. M.; Egorov, G. I.; Kolker, A. M. Density and Volumetric Properties of Aqueous Solutions of Trimethylamine N-Oxide in the Temperature Range from (278.15 to 323.15) K and at Pressures up to 100 MPa. Journal of Chemical & Engineering Data **2015**, 60, 1291–1299.

- (8) Knierbein, M.; Held, C.; Hölzl, C.; Horinek, D.; Paulus, M.; Sadowski, G.; Sternermann, C.; Nase, J. Density variations of TMAO solutions in the kilobar range: Experiments, PC-SAFT predictions, and molecular dynamics simulations. Biophysical Chemistry **2019**, *253*, 106222.
- (9) Sebastiani, F.; Verde, A. V.; Heyden, M.; Schwaab, G.; Havenith, M. Cooperativity and ion pairing in magnesium sulfate aqueous solutions from the dilute regime to the solubility limit. Phys. Chem. Chem. Phys. **2020**, *22*.
- (10) Shiraga, K.; Tanaka, K.; Arikawa, T.; Saito, S.; Ogawa, Y. Reconsideration of the relaxational and vibrational line shapes of liquid water based on ultrabroadband dielectric spectroscopy. Phys. Chem. Chem. Phys. **2018**, *20*, 26200–26209.
- (11) Hölzl, C.; Kibies, P.; Imoto, S.; Frach, R.; Suladze, S.; Winter, R.; Marx, D.; Horinek, D.; Kast, S. M. Design principles for high-pressure force fields: Aqueous TMAO solutions from ambient to kilobar pressures. J. Chem. Phys. **2016**, *144*, 144104.
- (12) Imoto, S.; Forbert, H.; Marx, D. Water structure and solvation of osmolytes at high hydrostatic pressure: pure water and TMAO solutions at 10 kbar versus 1 bar. Phys. Chem. Chem. Phys. **2015**, *17*, 24224–24237.
- (13) Marx, D.; Hutter, J. Ab Initio Molecular Dynamics: Basic Theory and Advanced Methods; Cambridge University Press, Cambridge 2009.
- (14) Hutter, J.; Iannuzzi, M.; Schiffmann, F.; VandeVondele, J. CP2K: atomistic simulations of condensed matter systems. Wiley Interdiscip. Rev. Comput. Mol. Sci. **2014**, *4*, 15–25.
- (15) Imoto, S.; Forbert, H.; Marx, D. Aqueous TMAO solutions as seen by theoretical THz spectroscopy: hydrophilic versus hydrophobic water. Phys. Chem. Chem. Phys. **2018**, *20*, 6146–6158.

- (16) Imoto, S.; Kibies, P.; Rosin, C.; Winter, R.; Kast, S. M.; Marx, D. Toward Extreme Biophysics: Deciphering the Infrared Response of Biomolecular Solutions at High Pressures. Angew. Chemie - Int. Ed. **2016**, 55, 9534–9538.